

Effects of Atomic Disorder on Carrier Transport in Si Nanowire Transistors

Hideki Minari^{*‡}, Tomofumi Zushi[†], Takano Watanabe^{†‡}, Yoshinari Kamakura^{*‡}, and Nobuya Mori^{*‡}

^{*}Graduate School of Engineering, Osaka University, 2-1 Yamada-oka, Suita City, Osaka 565-0871, Japan

[†]Faculty of Science and Engineering, Waseda University, Shinjuku, Tokyo 169-8555, Japan

[‡]CREST, Japan Science and Technology Agency, Chiyoda, Tokyo 102-0075, Japan

Email: minari@si.eei.eng.osaka-u.ac.jp

Abstract—Effects of oxidation-process-induced atomic disorder on extended electronic states in the channel region of narrow Si nanowire (NW) field-effect-transistors (FETs) are theoretically investigated by using the molecular dynamics, empirical tight-binding, and non-equilibrium Green's function methods. Simulation results show that the injection velocity in n-type Si NW FETs is less affected by the disorder compared to p-type devices, which can be attributed to differences in the in-plane carrier profile.

I. INTRODUCTION

Nanowire (NW) field-effect-transistors (FETs) are considered to be one of the most promising device structures that provide effective gate control even at the nanoscale. For narrow NWs with a diameter less than 10 nm, the overall mobility degradation is observed [1], whose origin has not been fully understood yet. One of the possible mechanisms associated with this degradation is due to atomic disorder existing near the Si/SiO₂ interfaces [2]. It causes localized states near the interfaces and modifies extended electronic states in the channel region. In our previous study [3], we have studied effects of the atomic-disorder-induced localized state and found that it significantly degrades the ballistic current in Si NW FETs. In the present study, we focus on effects of the atomic disorder on extended electronic states in Si NW FETs. We have numerically simulated carrier transport in oxidized Si NW FETs with realistic atomic disorder and investigated how it modifies the extended electronic states and affects the transport characteristics. We have constructed atomic structure models of the oxidized Si NWs by using a molecular dynamics (MD) method [4], [5]. Based on the models, we have calculated band structures and carrier distribution in Si NW FETs by using an empirical tight-binding (TB) approximation [6], [7] and the non-equilibrium Green's function (NEGF) formalism [8]–[10].

II. SIMULATION METHOD

A. Atomic Structure Models

Realistic atomistic structure models of oxidized Si NWs are constructed by the MD method with an empirical interatomic potential function carefully designed for Si and O mixed systems [5], [11]. The MD oxidation simulation is started from a pure Si NW with a diameter of 8 nm. The oxide films are constructed by two steps: (1) O atoms are inserted into the

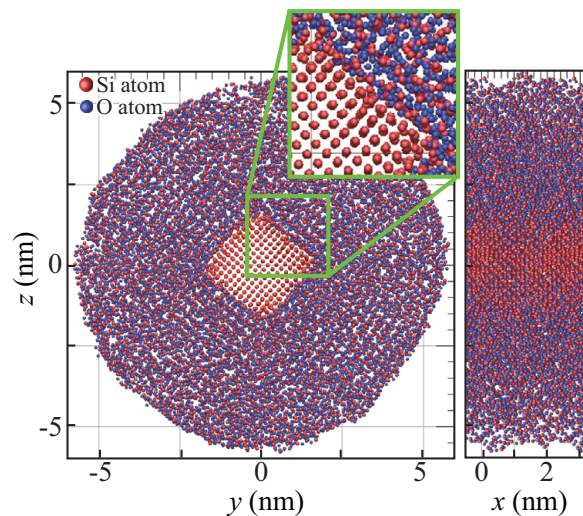


Fig. 1. Realistic atomic structure model of a Si NW created through MD oxidation simulation. The pure Si NW with an initial diameter of 8 nm is oxidized by 14 layers remaining a Si core region with $w = 2.7$ nm.

mid-points of Si-Si bonds for the outermost atomic layer; (2) the whole structure is annealed by the MD simulation with a temperature of 1,143 K. By repeating these processes, the atomic structure models of the oxidized Si NWs are obtained. Figure 1 shows the obtained atomic structure model of the Si NW oxidized by 14 layers. In the transport direction (x -direction), a periodic boundary condition with a period of 2.7 nm is applied. The Si NW has [100] crystal orientation along the NW axis (x -axis). The realistic NW structure obtained from the MD simulation has the atomic disorder near the Si/SiO₂ interface.

B. Band Structures and Carrier Distributions

The full-band structure is calculated by using an empirical $sp^3d^5s^*$ nearest-neighbor TB approximation without the spin-orbit coupling [12]. To treat realistic atomic structures within the framework of the TB method, atomic configuration models are constructed by just cutting Si cores out of the MD results. Figures 2(a) and (b) show the atomic configuration models of the Si NWs oxidized by 14 and 12 layers. The widths of Si core regions w are 2.7 nm and 3.5 nm for the Si NWs oxidized by 14 and 12 layers, respectively. We cut out the Si core

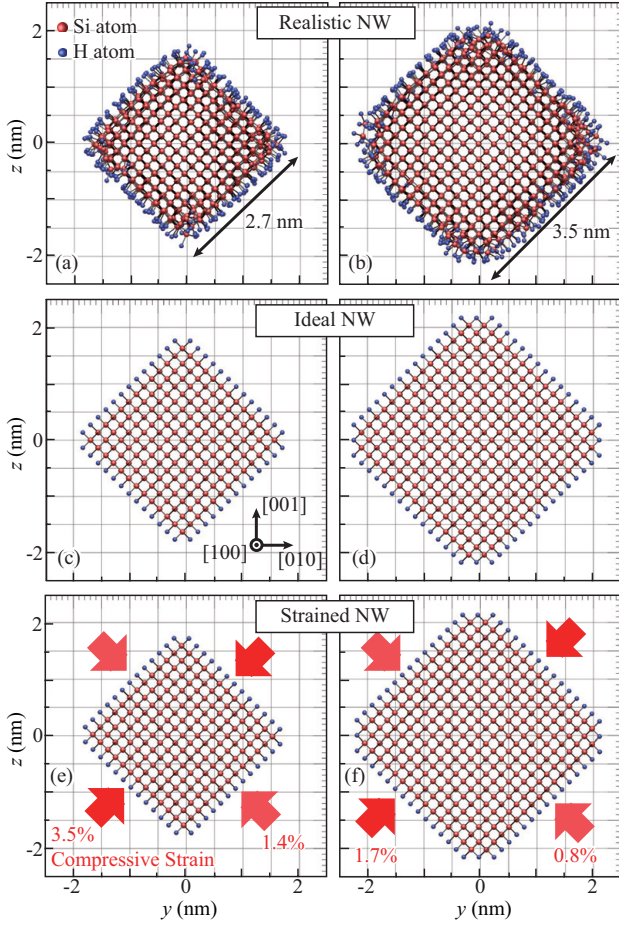


Fig. 2. Atomic structure models of Si NWs. Realistic NWs with (a) $w = 2.7$ nm and (b) 3.5 nm. (c) and (d) are the corresponding ideal NWs. (e) and (f) are the uniformly strained NWs with the average compressive strain.

by cutting the Si-Si bonds with a bond length $d > 1.03d_0$, where d_0 is the bond length of a pure Si crystal. In this condition, no defect-induced localized states remains in the Si core. For all the dangling bonds, the H termination model is used to eliminate artificial surface states in the energy region of interest [13]. The atomic structure models obtained from the MD oxidation can be directly applied to the TB method because the basis set in the TB method consists of atomic orbitals. For comparison, an ideal NW model without the atomic disorder is also constructed (see Figs. 2(c) and (d)). Figure 3 shows the strain distributions for the oxidized Si NWs, indicating a compressive strain is induced in the Si core region. For the Si NW with $w = 2.7$ nm, the average strain obtained from the Fourier analysis is 3.5% and 1.4% in [011]- and [0 $\bar{1}$ 1]-direction, respectively. Similarly, for the Si NW with $w = 3.5$ nm, the average strain is 1.7% and 0.8% in [011]- and [0 $\bar{1}$ 1]-direction, respectively. In order to separate the effects of the atomic disorder and the average strain, uniformly strained NW models based on the average strain observed in the realistic NW models are also constructed (see Figs. 2(e) and (f)).

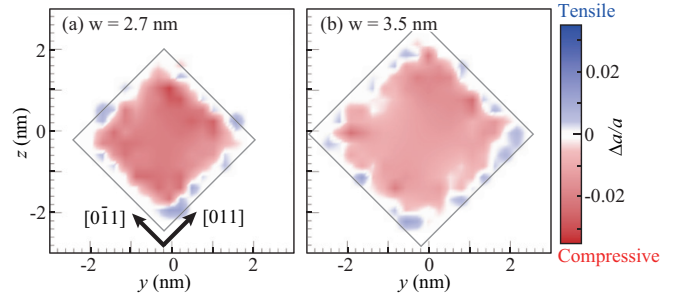


Fig. 3. Strain distribution for the oxidized Si NWs with (a) $w = 2.7$ nm and (b) 3.5 nm. Δa is a change of lattice constant and a is the lattice constant of a pure Si crystal.

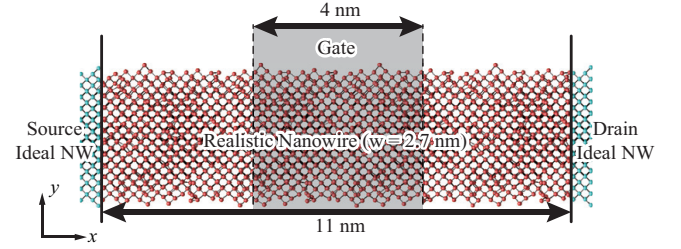


Fig. 4. Schematic diagram of a gate-all-around Si NW FET structure.

The carrier distribution in the NW FETs is calculated by the NEGF method [14]. We consider a gate-all-around NW FET with a gate-length of 4 nm and SiO₂-thickness of 1 nm (see Fig. 4). The channel is the realistic NW with a length of 11 nm constructed by repeating the oxidized NW model. The source and the drain contacts consist of the ideal Si NWs without the disorder. To compare the device performance between the n-type and the p-type devices, we assume that the gate consists of a fictitious metal whose Fermi level coincides with the lowest subband level of the NW. The doping concentration in the source and the drain regions, each of which is 3.5 nm long, is 5×10^6 cm⁻³. In the present study, we neglect scattering and assume ballistic transport. The potential profiles are obtained through a self-consistent solution of three-dimensional Poisson and NEGF equations.

III. RESULTS AND DISCUSSION

Figure 5 shows the subband structures for the conduction band. The energy zero is chosen to be the lowest subband level at $k_x = 0$. We find that the subband structure of the realistic NW is quite different from those of the ideal NW and the strained NW. This indicates that the atomic disorder has stronger impacts on the subband structures compared to the uniform strain. In the ideal NWs, there are four closely separated subbands near the band edge, where the second lowest subband is doubly degenerate. The origins of these four subbands are X valley states along the [010]- and [001]-direction in the bulk band structure. Because of a good symmetry of the ideal NWs, confinement energies for the X valley states are almost equal in the ideal NWs, which results in the small energy separation between the four subband states.

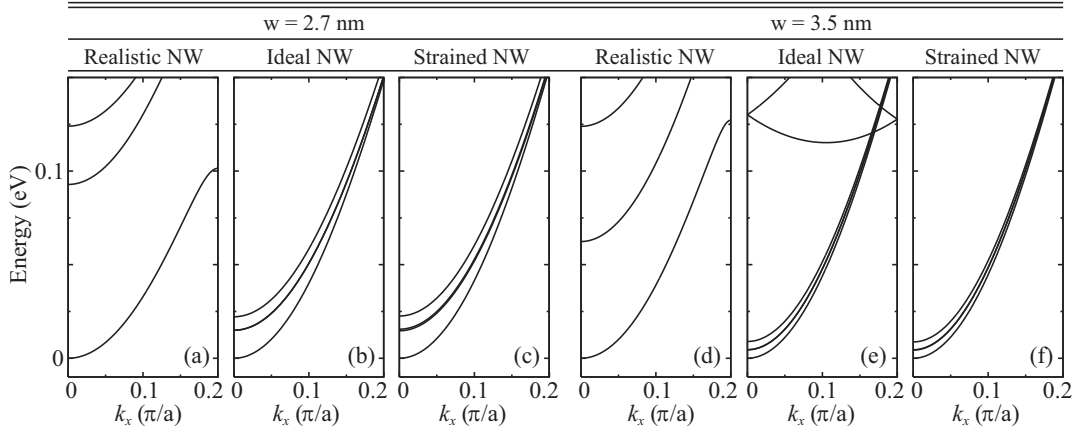


Fig. 5. Conduction subband dispersion for the realistic NWs with (a) $w = 2.7$ nm and (b) 3.5 nm. (c) and (d) correspond to the ideal NWs with the same sizes. (e) and (f) correspond to the uniformly strained NWs.

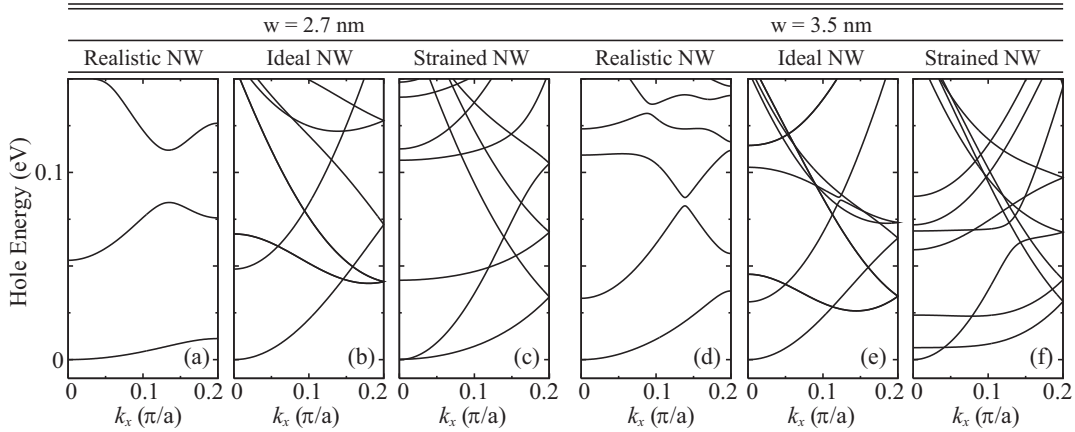


Fig. 6. The same as Fig. 5 but for the valence band.

On the other hand, for the realistic NWs, the subband spacings become larger because the disorder breaks the symmetry of the structure. The effective mass of the lowest conduction subband is found to be nearly independent of the disorder. As a result, the density-of-states (DOS) of the realistic NW becomes smaller compared to the ideal NW in the lower energy region.

Figure 6 shows the subband structures for the valence band. We find that the valence subband structure for the thinner NW with $w = 2.7$ nm is more strongly affected by the disorder compared to the thicker NW with $w = 3.5$ nm. The effective mass of the lowest subband of the realistic NW becomes much heavier especially for the thinner NW with $w = 2.7$ nm. These features can be understood by considering two types of holes. For the ideal NWs, the energy minimum of the lowest subband locates at $k_x = 0$ (we call this subband "Γ valley subband" hereinafter), while those of some higher subbands locate at off $k_x = 0$ (we call these subbands "off-Γ valley subbands" hereinafter). Figure 7 shows probability distributions for the Γ and the off-Γ valley states in the ideal NWs. For the thicker NW with $w = 3.5$ nm, the Γ valley state concentrates at the center, while the off-Γ valley states are distributed more

uniformly. Since the probability density of the off-Γ valley states is larger than that of the Γ valley state near the Si/SiO₂ interfaces where the disorder is present, the disorder mainly affects the off-Γ valley states. As a result, near the band edge, the effects of the disorder on the valence subband structure become small for $w = 3.5$ nm. On the other hand, for the thinner NW with $w = 2.7$ nm, both the Γ valley and the off-Γ valley states are distributed in the entire cross section because of the narrow NW width. Therefore, the Γ valley and the off-Γ valley states are mixed by the disorder near the interface, resulting in the heavy effective mass of the lowest subband for $w = 2.7$ nm.

To evaluate the FET performance, we have calculated the injection velocity, v_{inj} , from the band structures. Figure 8 shows v_{inj} as a function of carrier density, n . Although the slope near $n \sim 0$ becomes steeper when the disorder presents in n-type devices, there is no significant difference between the realistic and the ideal n-type NWs because of the similar effective masses of the both structures. Note that the change in the slope can be attributed to the smaller DOS of the realistic NWs. As for holes, a pronounced reduction of v_{inj} is

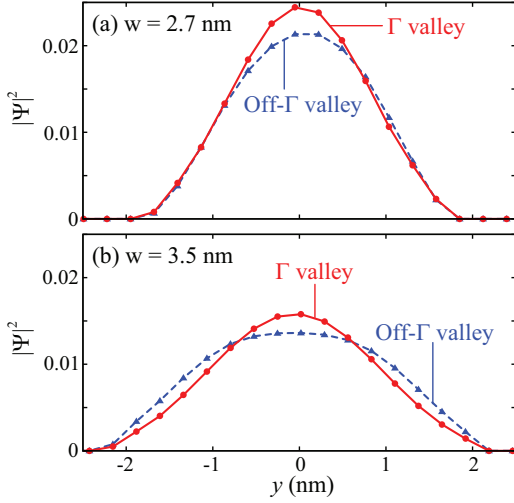


Fig. 7. Probability distribution in the cross section of the ideal NWs with (a) $w = 2.7$ nm and (b) 3.5 nm at $z = 0$. Solid lines show the results for the Γ valley state and dashed lines for the off- Γ valley states.

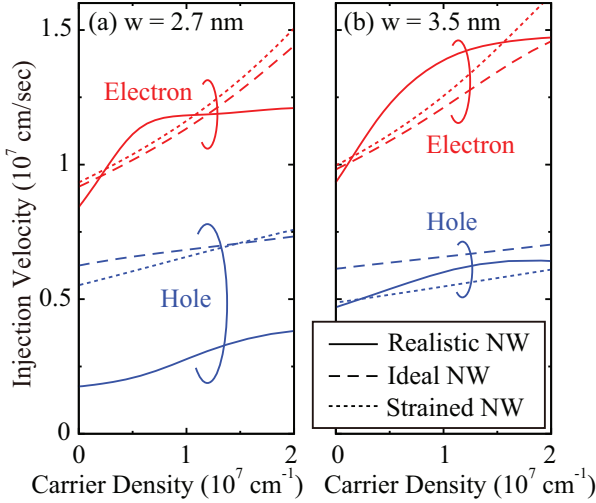


Fig. 8. Injection velocities for the NWs with (a) $w = 2.7$ nm and (b) $w = 3.5$ nm. Solid lines are the realistic NWs, dashed lines the ideal NWs, and dotted lines the strained NWs.

observed only for $w = 2.7$ nm, which reflects the fact that the Γ valley and the off- Γ valley states are mixed by the disorder for $w = 2.7$ nm. The differences in the effects of the disorder on the v_{inj} between the n-type and the p-type devices can be understood by observing the carrier distributions in the NW FETs. Figure 9 shows the carrier density profiles for the NW FETs with $w = 2.7$ nm. For the p-type device, the holes are distributed in the entire cross section and are easily affected by the disorder. On the other hand, for the n-type device, the electrons are distributed near the center and are less affected by the disorder near the Si/SiO₂ interface.

IV. CONCLUSION

We simulated transport characteristics in Si NW FETs with realistic atomic disorder by using the molecular dynamics,

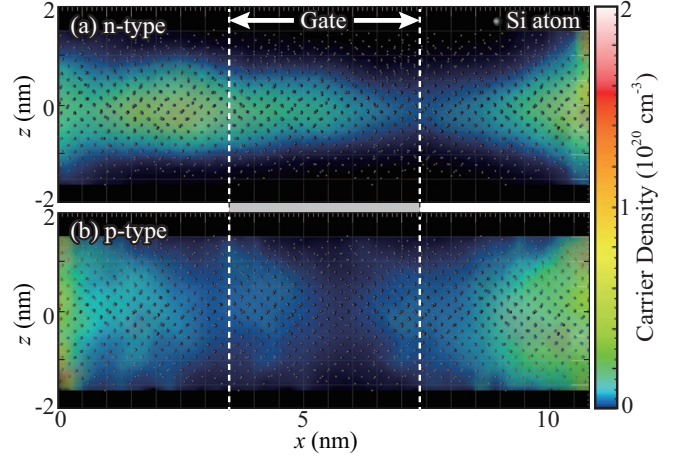


Fig. 9. Carrier density profiles for (a) n-type and (b) p-type devices at $V_G = 0$ V, $V_D = 0.2$ V, and $T = 300$ K.

empirical tight-binding, and non-equilibrium Green's function methods. The injection velocity in the n-type devices is found to be less affected by the disorder compared to the p-type devices, which can be attributed the fact that holes are distributed in the entire cross section and are easily affected by the atomic disorder.

REFERENCES

- [1] J. Chen, T. Saraya, K. Miyaji, K. Shimizu, and T. Hiramoto, "Experimental study of mobility in [110]- and [100]-directed multiple silicon nanowire GAA MOSFETs on (100) SOI," Proc. 2008 Symp. VLSI Tech., 32, 2008.
- [2] R. Haight and L.C. Feldman, "Atomic structure at the (111) SiSiO₂ interface," *J. Appl. Phys.*, vol. 53, 4884, 1982.
- [3] H. Minari, T. Zushi, T. Watanabe, Y. Kamakura, S. Uno, and N. Mori, "Impact of Oxidation Induced Atomic Disorder in Narrow Si Nanowires on Transistor Performance," Proc. 2011 Symp. VLSI Tech., 122, 2011.
- [4] F.H. Stillinger and T.A. Weber, "Computer simulation of local order in condensed phases of silicon," *Phys. Rev. B*, vol. 31, 5262, 1985.
- [5] T. Watanabe, H. Fujiwara, H. Noguchi, T. Hoshino, and I. Ohdomari, "Novel Interatomic Potential Energy Function for Si, O Mixed Systems," *Jpn. J. Appl. Phys.*, vol. 38, L366, 1999.
- [6] J.C. Slater and G.F. Koster, "Simplified LCAO Method for the Periodic Potential Problem," *Phys. Rev.*, vol. 94, 1498, 1954.
- [7] P.O. Löwdin, "On the Non-Orthogonality Problem Connected with the Use of Atomic Wave Functions in the Theory of Molecules and Crystals," *J. Chem. Phys.*, vol. 18, 365, 1950.
- [8] S. Datta, *Electronic Transport in Mesoscopic Systems*, Cambridge University Press, Cambridge, U.K., 1995, p. 293.
- [9] H. Haug and A.-P. Jauho, *Quantum Kinetics in Transport and Optics of Semiconductors*, Springer, Berlin, 1996, p. 35.
- [10] A. Di Carlo, "Tight-binding methods for transport and optical properties in realistic nanostructures," *Physica B*, vol. 314, 211, 2002.
- [11] T. Onda, T. Watanabe, and I. Ohdomari, "Crystal Orientation Dependency of Oxidation-Induced Strain in Silicon Nanostructures: A Molecular Simulation Study," ISSS-5, Tokyo, Japan, 2008.
- [12] Y.M. Niquet, D. Rideau, C. Tavernier, H. Jaouen, and X. Blase, "Onsite matrix elements of the tight-binding Hamiltonian of a strained crystal: Application to silicon, germanium, and their alloys," *Phys. Rev. B*, vol. 79, 245201, 2009.
- [13] S. Lee, F. Oyafuso, P. von Allmen, and G. Klimeck, "Boundary conditions for the electronic structure of finite-extent embedded semiconductor nanostructures," *Phys. Rev. B*, vol. 69, 045316, 2004.
- [14] H. Minari, T. Kitayama, M. Yamamoto, and N. Mori, "Strain Effects on Hole Current in Silicon Nanowire FETs," Proc. SISPAD, 207, 2010.